

# On Transmissive RIS for mm-Waves Outdoor-to-Indoor Coverage Enhancement

Silvi Kodra\*, Simone Del Prete\*, Elena Bernardi\*, Franco Fuschini\*, Marina Barbiroli\*,  
Enrico Maria Vitucci\*, Vittorio Degli-Esposti\*

\*Department of Electrical, Electronic and Information Engineering “G. Marconi,” CNIT, University of Bologna, Italy

**Abstract**—This paper investigates the use of large Reconfigurable Intelligent Surfaces (RIS), also known as “Smart Skins”, to improve outdoor-to-indoor millimetre-wave (mmWave) propagation, taking advantage of ventilation holes commonly found, or easily realizable, in European buildings. By using a transmissive, focusing RIS, the signal could be concentrated and routed through the opening, enhancing signal penetration into the indoor space even in modern, highly insulated buildings that particularly hinder signal penetration. Using Ray tracing simulations at 27 GHz we compare scenarios with and without RIS, demonstrating significant indoor signal coverage improvements in the first case. The study highlights the use of RIS - or smart-skins - as a cost-effective solution to address the challenges of mmWave propagation in modern building designs.

**Index Terms**—Outdoor-to-Indoor propagation, Ray Tracing, transmissive RIS.

## I. INTRODUCTION

A key trend in “5G and beyond” technology lies in the utilization of high-frequency bands, particularly millimetre-wave (mm-wave) frequencies in the range of 27 GHz and above. These bands offer access to vast amounts of undivided spectrum, enabling unprecedented data rates and enhancing the quality of service for a wide range of applications. However, a significant challenge associated with mm-wave signals is their poor through-material penetration capabilities, resulting in severe path loss and thus severely limiting link range in indoor and outdoor-to-indoor (O2I) applications [1]. Ensuring good indoor connectivity at mm-waves has therefore become a critical concern, particularly considering that most high-data rate applications take place indoor and modern buildings use thermal and acoustical insulation solution that further hinders signal penetration. Several innovative approaches are being explored to address these issues. Advanced beam-forming techniques, network densification, the incorporation of active repeaters and antenna-embedded walls [2] [3] are among the proposed solutions. However, one promising solution that has gained significant attention is the use of Reconfigurable Intelligent Surfaces (RIS) [4] [5].

A RIS is an artificial two-dimensional thin structure composed of a substrate with a distribution of electrically small metal or dielectric patches printed on it [6]. The shape and size of these patches vary across the surface to achieve a desired effect on the wavefront of the re-radiated wave [7]. By manipulating the phase, amplitude, and polarization of the reradiated wave, RIS enables functionalities that were previously unattainable with natural materials. The real-time

reconfigurability of RIS is made possible through the integration of tunable devices [8] [9], positioning RIS-assisted networks as a key technology in future 6G systems [10]. RIS can either anomalously reflect or transmit (refract) waves based on its configuration. In a reflective RIS, the surface re-radiates the wave towards the intended user when both the base station (BS) and user are on the same side. In contrast, transmissive RIS is used to transmit a wave through the surface when the BS and user are located on opposite sides, such as in outdoor-to-indoor scenarios [11]. Although the transmissive mode might be important for improving indoor coverage, much of the existing research has primarily focused on reflective RIS [12]. Only recent studies have started to investigate transmissive RIS and their potential to enhance indoor coverage [13]–[15]. When strategically positioned on walls or windows, transmissive RIS can concentrate and reroute the signal through openings toward the desired spot, thereby mitigating signal blockage and offering a promising solution to indoor coverage challenges.

Building on previous work on macroscopic modelling of metasurfaces, here the model in [16] is extended to account for spherical wave incidence. Moreover, an evaluation of outdoor-to-indoor coverage with and without RIS is performed using the foregoing model in a simple reference case.

## II. TRANSMISSIVE RIS: EXTENDED MATHEMATICAL MODELING

In the reference model developed in [16], the RIS is viewed as a two-dimensional array of antenna elements. Specifically, the surface is divided into elements of area  $\Delta S$ , each of which can be seen as an aperture antenna that receives an incident power  $P_i$  and re-radiates a wave with power  $P_m$  (see [16], [17] for more details). RIS is composed by  $N_X \times N_Y$  antenna elements and the position in space of a generic  $n$ -th element is defined by the coordinates  $(x_n, y_n) = (\Delta l \cdot u, \Delta l \cdot v)$ , where  $\Delta l$  represents the distance between the individual elements of the RIS ( $\simeq \lambda/2$ ), and  $(u, v)$  are the indices identifying them. The reference system used for this work is shown in Fig.1. RIS is positioned in the  $XY$  plane with its center located at the origin. The position of the transmitter (Tx) and receiver (Rx) is defined using spherical coordinates:  $(\theta_{i,r}, \phi_{i,r}, d_{Tx,Rx})$  where the angles  $\theta_i, \phi_i$  and  $\theta_r, \phi_r$  represent the direction (with respect to the center of the RIS) of incidence and re-radiation respectively.  $d_{Tx}$  is the Tx-RIS distance and  $d_{Rx}$  is the Rx-RIS distance.

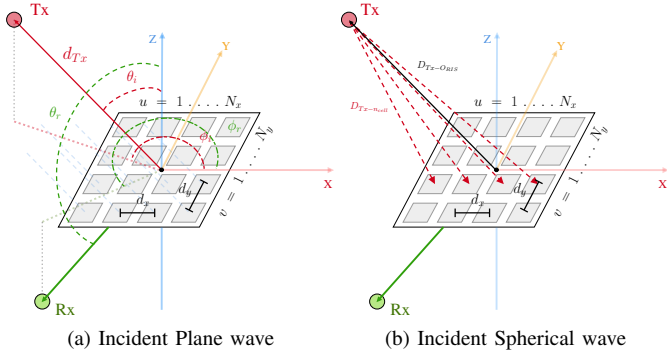


Fig. 1: Reference scheme for an RIS illuminated by an incident wave. In 1a, under plane wave incidence, the traveled distance from the Tx to each RIS element is identical. Instead, in the spherical wave scenario described in 1b, the traveled distance varies for each RIS element.

Since RIS aims to re-radiate the incident wave in a desired direction by reducing specular reflection and scattering, it imposes a certain spatial modulation (in amplitude and phase) on the incident wave. In order to obtain the phase shift of the RIS for a given functionality, first, phase shifts of the incident and desired re-radiated wave need to be known. The phase of the wave incident on a generic  $n$ -th element of the RIS is expressed in (1) for the case of an incident plane wave.

$$\chi_{ipw} = \beta \sin(\theta_i) (x_n \cos(\phi_i) + y_n \sin(\phi_i)), \quad (1)$$

where  $\beta$  is the wavenumber. Referring to Fig. 1, (1), is obtained considering the spatial phase differences between adjacent antenna elements along the  $x$ -axis  $\Delta\chi_x$  and  $y$ -axis  $\Delta\chi_y$  as follows:

$$\Delta\chi_x = \beta u d_x \sin(\theta_i) \cos(\phi_i), \quad (2)$$

$$\Delta\chi_y = \beta v d_y \sin(\theta_i) \sin(\phi_i), \quad (3)$$

where  $u \in 1, \dots, N_x$  and  $v \in 1, \dots, N_y$ .

In scenarios where the Tx is positioned within the near field of the RIS, the phase of the incident spherical wave is considered, as illustrated in Fig. 1b, and given as:

$$\chi_{isw} = -\beta d_{nTx}, \quad (4)$$

where  $d_{nTx}$  is the distance between Tx and  $n$ -th element of the RIS.

Moreover, the phase of the re-radiated wave is calculated based on desired RIS functionality and can be distinguished as:

- 1) the case where RIS works as an anomalous reflector and therefore the re-radiated wave is planar. The phase of the re-radiated wave is expressed by:

$$\chi_r = -\beta \sin(\theta_r) (x_n \cos(\phi_r) + y_n \sin(\phi_r)) \quad (5)$$

- 2) the case where RIS works as a focusing lens at a desired near-field reception point. The phase of the re-radiated wave in this case is given by (6):

$$\chi_{rfocus} = -\beta d_{Rx} \quad (6)$$

Therefore, the phase of the spatial modulation coefficient associated with the  $n$ -th element of the RIS for a desired functionality is calculated through the difference between the phase of the re-radiated wave and the phase of the incident wave, as expressed in (7):

$$\chi_{RIS} = \chi_{re-radiated} - \chi_{incident}, \quad (7)$$

where  $\chi_{re-radiated}$  can be either  $\chi_r$  or  $\chi_{rfocus}$  depending on RIS functionality and  $\chi_{incident}$  can be either  $\chi_{ipw}$  or  $\chi_{isw}$  depending on if incident wave is plane or spherical.

After obtaining the phase shift generated by RIS, the bilateral power balance in [16] for all the re-radiation modes needs to be satisfied:

$$1 = R_R^2 \sum_{n=0}^N m_{R_n} + S_R^2 \sum_{n=0}^N m_{R_n} + R_T^2 \sum_{k=0}^K m_{T_k} + S_T^2 \sum_{k=0}^K m_{T_k} + \alpha \quad (8)$$

Here  $m_R$  and  $m_T$  are the re-radiation coefficients that determine the fraction of incident power that is re-radiated in one mode in reflection and transmission and  $\sum_{n=1}^N m_{R_n}$  and  $\sum_{k=1}^K m_{T_k}$  represent the total power re-radiated in the backward (reflection) and forward half-space (transmission), respectively.  $\alpha$  is the dissipation parameter that accounts for the percentage of the dissipated power on the substrate and  $R_{T,R}$  and  $S_{T,R}$  are the Rayleigh and diffuse scattering coefficients respectively. In the summations above, the indices  $n=0$  and  $k=0$  indicate the specular propagating modes.

Once the power balance is satisfied, the total re-radiated field is calculated as the sum of all propagating modes :

$$E_{tot}(P) = \sum \sum \Delta E_m(P|x_n, y_n) \quad (9)$$

where  $P$  represents the position of the receiver.

### III. USE CASE AND DISCUSSION

To evaluate the impact of RIS on indoor coverage, here the authors propose to take advantage of the ventilation holes commonly found in European buildings. A comparative study using ray tracing (RT) simulations at 27 GHz in an outdoor-to-indoor scenario is conducted, examining two cases: one without RIS and one with RIS. The detailed parameters of the simulations are given in Table I.

#### A. Case Without RIS:

In the first scenario, the RT simulation between Tx and Rx was performed without the presence of RIS. The Tx was placed in the far field, illuminating the external wall of a building composed of a room only (for simulation overhead reduction). A dense grid of receivers was placed inside the room in order to obtain insights on the received power all across the room. The external wall is a brick wall with its permittivity and conductivity taken from [18]. A central ventilation hole is present in the external wall, representing a

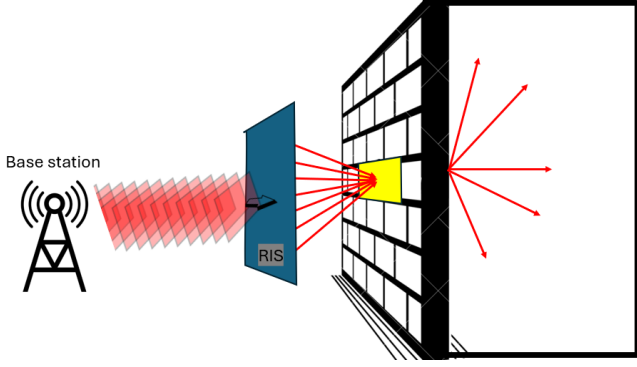


Fig. 2: Schematic simulation scenario with RIS

realistic case. The aim of this simulation was to assess signal penetration through the wall and its distribution into the indoor environment. Fig. 3 shows the received power inside the room at a height of  $1m$  from the ground which is a typical user height. As seen from Fig. 3 it was confirmed that indoor received power in case of no RIS was notably low, with a higher received power only in the region directly in front of the ventilation hole, which is a result of the direct ray entering the ventilation hole from the Tx. The high attenuation is due to the high attenuation of the external wall itself at 27 GHz.

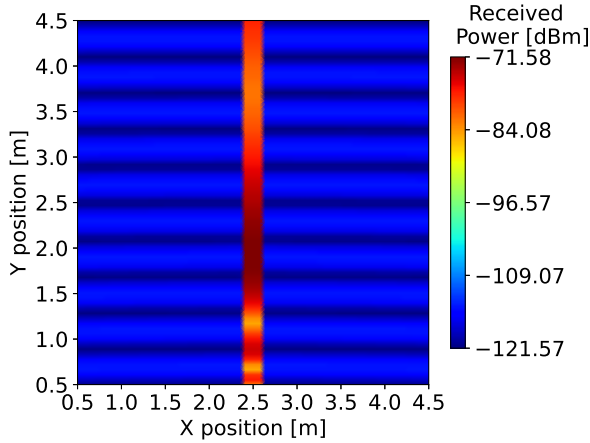


Fig. 3: Indoor coverage without RIS

### B. Case With RIS

In the second scenario, a RIS was integrated into the RT tool, combining it with the model described in Section II. The RIS used for this use case is not re-configurable: it is a fixed functionality "Smart Skin" with a very low cost. The characteristics of the RIS are summarized in Table I. The proposed approach exploits small ventilation holes commonly found in most European buildings by placing a focusing RIS on the external part of the wall. Thanks to the phase profile generated according to Section II, the RIS is assumed to collect the impinging power and to focus it toward the center of the ventilation hole, using a focusing efficiency value obtained from the literature [19]. After propagation through

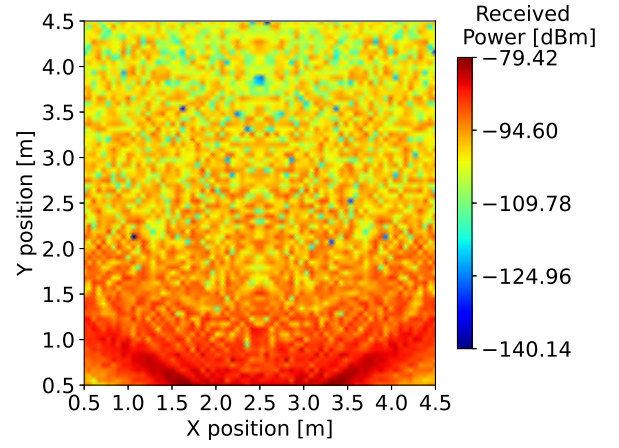


Fig. 4: Indoor coverage with RIS

the hole (properly coated with a metal film waveguide) the wave spreads into the indoor environment, therefore offering enhanced coverage compared to the scenario without RIS. The simulation scenario is illustrated in a schematic way in Fig. 2. The dimensions of the RIS, the ventilation hole, and the focusing distance from the RIS surface were chosen with careful consideration in order to reflect realistic conditions and practical fabrication limitations for a low-cost RIS realization (refer to Table I for more details). However, it is important to mention that with very advanced manufacturing techniques, much larger Smart Skins (even  $2m^2$ ) could be produced, leading to greater efficiency. Fig. 4 shows the received power distribution at a height of  $1m$  from the ground when RIS is used.

It can be observed that RIS effectively spreads coverage into the room in a fan-shaped area, creating a well covered region (around  $-79$  dBm) near the center of the  $x$ -coordinate of the room that is aligned with the position of the ventilation hole. As expected, power decreases with distance from the focal point, showing a smooth gradient toward the edges of the room. Fig. 5 shows the Cumulative Distribution Functions (CDF) obtained from the 3D grid of receivers all across the room. It can be observed that in the case with RIS, the overall received power is several dB higher and more uniform across the environment. On the contrary, without RIS, coverage is confined to the area directly aligned with the ventilation hole, where the direct path from the BS exists. This is reflected by the higher probability of receiving power below  $-180$  dBm. At high CDF values, the curves converge because those correspond to receiver points directly after the ventilation hole, where the direct Tx-Rx rays dominate and the gain of the RIS becomes negligible compared to the strong direct signal.

The main focus of this study is to propose a new approach to indoor coverage improvement by the aid of a RIS and to compare performance in a simple case with and without the integration of RIS. Looking ahead, the development of modern buildings with low thermal emission and highly insulating materials is expected to further hinder millimeter-wave prop-

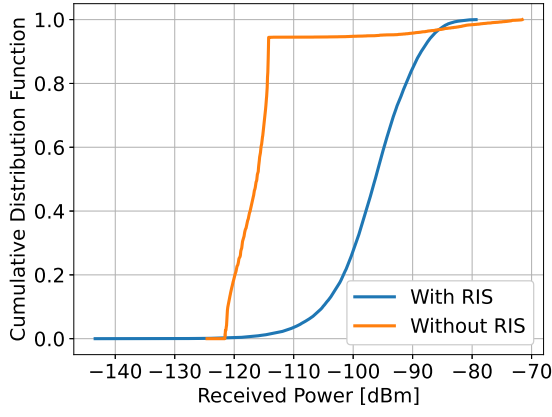


Fig. 5: Power CDF in the two scenarios: with and without the RIS

TABLE I: Simulation parameters

Parameter	Values
Tx height	4 m
Tx power	10 dBW
Tx antenna gain	10 dBi
Rx antenna	Omnidirectional
Tx-external wall distance	250 m
Incident wave	Plane, $0^\circ$
Frequency	27 GHz
Polarization	Vertical
Room size	5m x 5m x 3m
RIS dimension	1m x 1m
Ventilation hole dimension	0.1m x 0.1m
RIS Focusing distance	0.1m
RIS efficiency	25%
$\epsilon_r$ external wall	5.4
$\sigma$ external wall	0.4 S/m
Thickness external wall	0.25 m

agation. As a result, the use of RIS or smart-skin technology can be considered a promising and cost-effective solution to mitigate these future propagation issues and enhance indoor signal penetration.

#### IV. CONCLUSIONS

In this work, a previously proposed macroscopic model for metasurfaces is extended to account for spherical wave incidence, integrated into a ray tracing tool and used to assess outdoor-to-indoor coverage with the aid of a RIS. We observe that, by strategically placing a focalizing RIS over a ventilation hole, indoor coverage can be improved on average by several dB. Other application cases, more realistic scenarios as well as the synthesis of the proper RIS microstructure to realize large smart skins with low focal length, will be addressed in follow-on studies.

#### ACKNOWLEDGMENT

This work was supported in part by the European Union - Next Generation EU under the Italian National Recovery and Resilience Plan (NRRP), Mission 4, Component 2, Investment 1.3, partnership on “Telecommunications of the Future” (PE00000001 - program “RESTART”), in part by the

Eu Project 6G-SHINE (6G SHORT range extreme communication IN Entities), Horizon Europe Programme, Grant No. 101095738, and in part by the EU COST Action INTERACT (Intelligence-Enabling Radio Communications for Seamless Inclusive Interactions), Grant CA20120.

#### REFERENCES

- [1] S. Kodra, M. Barbiroli, E. M. Vitucci, F. Fuschini, and V. Degli-Esposti, “Mm-wave building penetration losses: A measurement-based critical analysis,” *IEEE Open Journal of Antennas and Propagation*, vol. 5, no. 2, pp. 404–413, 2024.
- [2] L. Vähä-Savo, K. Haneda, C. Icheln, and X. Lü, “Electromagnetic-thermal analyses of distributed antennas embedded into a load-bearing wall,” *IEEE Transactions on Antennas and Propagation*, vol. 71, no. 8, pp. 6849–6858, 2023.
- [3] L. Vähä-Savo, L. Veggi, E. M. Vitucci, C. Icheln, V. Degli-Esposti, and K. Haneda, “Analytical characterization of a transmission loss of an antenna-embedded wall,” *IEEE Open Journal of Antennas and Propagation*, pp. 1–1, 2024.
- [4] D. Kitayama, Y. Hama, K. Goto, K. Miyachi, T. Motegi, and O. Kagaya, “Transparent dynamic metasurface for a visually unaffected reconfigurable intelligent surface: controlling transmission/reflection and making a window into an RF lens,” *Opt. Express*, vol. 29, no. 18, pp. 29 292–29 307, Aug 2021. [Online]. Available: <https://opg.optica.org/oe/abstract.cfm?URI=oe-29-18-29292>
- [5] Z. Li, H. Hu, J. Zhang, and J. Zhang, “Coverage analysis of multiple transmissive ris-aided outdoor-to-indoor mmwave networks,” *IEEE Transactions on Broadcasting*, vol. 68, no. 4, pp. 935–942, 2022.
- [6] C. Simovski and S. Tretyakov, *An Introduction to Metamaterials and Nanophotonics*. Cambridge University Press, 2020.
- [7] M. Di Renzo, F. H. Danufane, and S. Tretyakov, “Communication models for reconfigurable intelligent surfaces: From surface electromagnetics to wireless networks optimization,” *Proceedings of the IEEE*, vol. 110, no. 9, pp. 1164–1209, 2022.
- [8] Y. Feng, Q. Hu, K. Qu, W. Yang, Y. Zheng, and K. Chen, “Reconfigurable intelligent surfaces: Design, implementation, and practical demonstration,” *Electromagnetic Science*, vol. 1, no. 2, pp. 1–21, 2023.
- [9] M. Merluzzi and A. Clemente, “Anomalous and specular reflections of reconfigurable intelligent surfaces: Configuration strategies and system performance,” *IEEE Wireless Communications Letters*, vol. 13, no. 10, pp. 2707–2711, 2024.
- [10] Z. Zhu and X. Huang, “Connectivity of wireless networks assisted by transmissive reconfigurable intelligent surfaces,” in *2023 IEEE 98th Vehicular Technology Conference (VTC2023-Fall)*, 2023, pp. 1–6.
- [11] S. Zeng, H. Zhang, B. Di, Y. Tan, Z. Han, H. V. Poor, and L. Song, “Reconfigurable intelligent surfaces in 6g: Reflective, transmissive, or both?” *IEEE Communications Letters*, vol. 25, no. 6, pp. 2063–2067, 2021.
- [12] W. Tang, M. Z. Chen, X. Chen, J. Y. Dai, Y. Han, M. Di Renzo, Y. Zeng, S. Jin, Q. Cheng, and T. J. Cui, “Wireless communications with reconfigurable intelligent surface: Path loss modeling and experimental measurement,” *IEEE Trans. Wireless Commun.*, vol. 20, no. 1, pp. 421–439, 2021.
- [13] J. Tang, M. Cui, S. Xu, L. Dai, F. Yang, and M. Li, “Transmissive ris for b5g communications: Design, prototyping, and experimental demonstrations,” *IEEE Transactions on Communications*, vol. 71, no. 11, pp. 6605–6615, 2023.
- [14] K. Goto, S. Suyama, T. Yamada, K. Arai, and O. Kagaya, “Experimental trials with combination of multiple transmissive metasurfaces and beamforming for mmw coverage enhancement,” in *2023 IEEE 98th Vehicular Technology Conference (VTC2023-Fall)*, 2023, pp. 1–5.
- [15] S. Danesh, A. Bagheri, and M. Khalily, “Wide-incidence angle and polarisation insensitive transparent metasurface for 5g outdoor to indoor coverage enhancement,” in *2022 IEEE International Symposium on Antennas and Propagation and USNC-URSI Radio Science Meeting (AP-S/URSI)*, 2022, pp. 239–240.
- [16] S. Kodra, E. M. Vitucci, M. Barbiroli, M. Albani, and V. Degli-Esposti, “A macroscopic bilateral modeling approach for reflective and transmissive metasurfaces,” in *2024 18th European Conference on Antennas and Propagation (EuCAP)*, 2024, pp. 1–4.

- [17] V. Degli-Esposti, E. M. Vitucci, M. D. Renzo, and S. A. Tretyakov, "Reradiation and scattering from a reconfigurable intelligent surface: A general macroscopic model," *IEEE Transactions on Antennas and Propagation*, vol. 70, no. 10, pp. 8691–8706, 2022.
- [18] I. T. U. ITU-R, Rec. ITU-R P.2040-2, "Effects of building materials and structures on radiowave propagation above about 100 MHz," Sept. 2021.
- [19] J. L. Wu, Y. M. Pan, and S. Y. Zheng, "Design of single-layer polarization-dependent transmissive and reflective focusing metasurface," *IEEE Transactions on Antennas and Propagation*, vol. 69, no. 11, pp. 7637–7646, 2021.